Vital Signs Monitoring of Multiple People using a FMCW Millimeter-Wave Sensor

Adeel Ahmad, June Chul Roh, Dan Wang, Aish Dubey

Texas Instruments Incorporated

12500 TI Boulevard,

Dallas, Texas, USA

Abstract—In this paper, we describe non-contact monitoring of vital signs of multiple people using a frequency modulated continuous wave (FMCW) sensor. We use the inherent range-gating ability of the FMCW waveforms and multiple receive channels to separate objects in range-azimuth plane. We subsequently utilize the fact that body surface movements due to physiological motions modulates the phase of the received radar signal and can be further processed to extract the breathing and heart-rate. Range-gating and beamforming techniques allow the signal of interest to be isolated from surrounding clutter, however several challenges such as random body movements need to be addressed before radar-based non-contact measurements can be deployed in real-world settings.

I. INTRODUCTION

Currently the main focus of mm-wave radar applications are geared towards the automotive market [1], however several potential application areas within the broad industrial and health-care domain are also under active investigation. Millimeter-wave radars are currently being explored for use in numerous medical and diagnostic applications ranging from cancer imaging to glucose monitoring [2]. One emerging application area is remote non-contact monitoring of human vital signs [3]. This can be important in several scenarios such as monitoring a room full of sleeping elderly or inebriated people to diagnose life threatening situations at low cost; in critically-ill patients where non-contact measurements might be more desirable such as in neonatal units for babies and for burn victims; for driver monitoring to detect driver drowsiness and sleepiness to avoid auto accidents; in detecting humans who are either buried in emergency accident situations or hiding to resolve a security situation etc.

In this paper, we demonstrate the feasibility of measuring human vital-signs of multiple people using a frequency modulated continuous wave (FMCW) CMOS mm-wave sensor operating from 76-81 GHz. We utilize the frequency modulated waveform and measurements over multiple receive channels to separate objects in the range-azimuth angle plane and further process the phase signal to extract the breathing-rate and heart-rate. We also demonstrate that these applications could be reliably supported by an integrated solution which helps in optimizing the size, power consumption and cost of the safety critical monitoring solutions. In section 2 of this paper, we briefly describe the vital signs signal model from a FMCW radar perspective and measurement of the displacement sensitivity of our system. In section 3, we explain the main processing steps to extract the breathing and heart-rate from multiple people within the radar field-of-view followed by a discussion on the current challenges and future work.

II. BACKGROUND

A. Signal Model

The FMCW signal model is described in detail in several previous studies [4]. Briefly, a periodic linearly-increasing frequency ramps are transmitted given by

$$x_T(t) = A_T \cos(2\pi f_c t + \pi \frac{B}{T_c} t^2 + \phi(t)) \tag{1}$$

where A_T is the transmitted power and $\phi(t)$ is the phase noise from the transmitter. Some relevant chirp parameters are defined as below

f_c: Chirp starting frequency

B: Bandwidth of the chirp

T_c: Chirp duration

T_f: Fast-time-axis ADC sampling interval

T_s: Slow-time-axis sampling interval

The radar receives a scaled and shifted (by α and t_d) version of the transmitted signal given by

$$x_R(t) = \alpha A_T \{\cos(2\pi f_c(t - t_d) + \pi \frac{B}{T_c}(t - t_d)^2 + \phi(t - t_d) \tag{2}$$

where $t_d = 2R(t)/c$ is the range-dependent time delay from a given object at radial range $R(t)$. The received signal is mixed with a replica of the transmitted signal and after I/Q mixing the signal can be approximated as

$$y(t) = A_R e^{j(2\pi[\frac{B}{T_c} t_d]t + 2\pi f_c t_d + \pi \frac{B}{T_c} t_d^2 + \Delta\phi(t))}$$
$$= A_R e^{j(2\pi f_b t + \phi_b(t) + \Delta\phi(t))} \tag{3}$$

where A_R is the received signal power, f_b is the beat frequency given by

$$f_b = \frac{2BR(t)}{cT_c}, \tag{4}$$

and

$$\phi_b(t) = 2\pi f_c t_d + \pi \frac{B}{T_c} t_d^2 \tag{5}$$

is the phase.

The residual phase noise is $(\Delta\phi(t) = \phi(t) - \phi(t - 2R/c))$ and can be negelcted for short-range radar applications due to

the range-correlation effect. Additionally, the term $\pi \frac{B}{T_c} t_d^2$ can also be neglected in ϕ_b as it is negligibly small in practical scenarios.

The beat signal after I/Q sampling can be expressed for the nth ADC sample and m^{th} chirp as

$$y[n,m] = A_R e^{j(2\pi f_b n T_f + \frac{4\pi}{\lambda} R(nT_f + mT_s))} \quad (6)$$

In a system with multiple receivers, an additional phase shift will occur due to the relative distances between the various receiver elements. For an object at angle, the signal received at receiver i that is placed at a relative distance d_i (assuming a uniform linear array) is

$$y[n,m,i] = A_R e^{j(2\pi f_b n T_f + \frac{4\pi}{\lambda} R(nT_f + mT_s) + \frac{2\pi}{\lambda} d_i \sin \theta)} \quad (7)$$

If multiple targets are present within the radar field-of-view, then the received signal is additive and for L number of targets at (R_l, θ_l) is given as below

$$y_T[n,m,i] = \sum_{l=1}^{L} A_{R_l} e^{j(2\pi f_{bl} n T_f + \frac{4\pi}{\lambda} R_l(nT_f + mT_s) + \frac{2\pi}{\lambda} d_i \sin \theta_l)} \quad (8)$$

Based on the above equation, the phase shift at the ith receiver is

$$\phi_{b,i}(nT_f + mT_s) = \frac{4\pi R_l(nT_f + mT_s)}{\lambda} + \frac{2\pi}{\lambda} d_i \sin \theta_l \quad (9)$$

Body surface displacement due to vital signs is of small amplitudes (< 10 mm) and low frequency (< 4 Hz). This implies that there would be no appreciable change in phase during the chirp time (fast-time axis) and measuring phase changes induced between successive chirps (slow-time axis) would be sufficient. If the object is at a nominal range $R_{l,o}$ then

$$R_l(nT_f + mT_s) \approx R_{l,o} + R_l(mT_s) \quad (10)$$

$$\phi_{b,i}(mT_s) = \frac{4\pi R_{l,o}}{\lambda} + \frac{4\pi R_l(mT_s)}{\lambda} + \frac{2\pi}{\lambda} d_i \sin \theta_l \quad (11)$$

$$= \phi_{c,i}(R_{l,o}, \theta) + \frac{4\pi R_l(mT_s)}{\lambda} \quad (12)$$

where $\phi_{c,i}(R_{l,o}, \theta_l)$ would be a constant for an object that remains in the same range-angle bin i.e. $(R_{l,o}, \theta_l)$. In vital signs measurement, we are mainly interested in the relative displacement, $R_l(mT_s)$ and hence the constant phase term is not considered, however, it can be seen that any changes in $(R_{l,o}, \theta_l)$ during the course of the measurements can significantly affect the results. The phase changes across the receivers are however utilized to monitor and analyze the vital signs for people that are in separately identifiable range-angle bins.

B. Displacement Sensitivity

Its apparent from the expression of ϕ_b that a smaller λ will generate a larger phase change for a given displacement $R(t)$. This explains why 77 GHz, millimeter-wave radars by virtue of their smaller wavelengths (≈ 3.9 mm), have greater sensitivity in measuring small displacements that can be as low as tens of microns due to heart beats. As we are using the phase to measure the vibrational amplitude and frequency, hence it is useful to characterize the phase sensitivity of the system. We define phase sensitivity as the RMS value of the phase fluctuations of a static object. Phase sensitivity of the system would determine the smallest observable/measurable change in phase that the system can measure and is related to the displacement sensitivity by $\sigma_R = \frac{\lambda}{4\pi} \sigma_\phi$
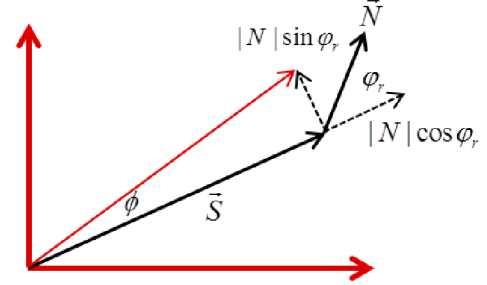

Fig. 1. Noise model for determining the phase sensitivity of the system

To derive, the theoretical curve for phase/displacement sensitivity we use a simplified noise model shown in Figure 1. The measured signal can be modelled as the summation of the ideal signal $\vec{S}$ and noise $\vec{N}$. Based on Figure 1, the phase variations ϕ due to noise in the measured signal can be approximated as $\tan \phi \approx \phi = \frac{|N| \sin \varphi_r}{|S|}$. Under the assumption that noise has a random phase φ_r uniformly distributed between 0 and 2π, the phase variance is given by $\sigma_\phi^2 = \frac{1}{2} \frac{|N^2|}{|S^2|} = \frac{1}{2(SNR)^2}$ and the RMS value is $\sigma_\phi = \frac{1}{\sqrt{2(SNR)}}$
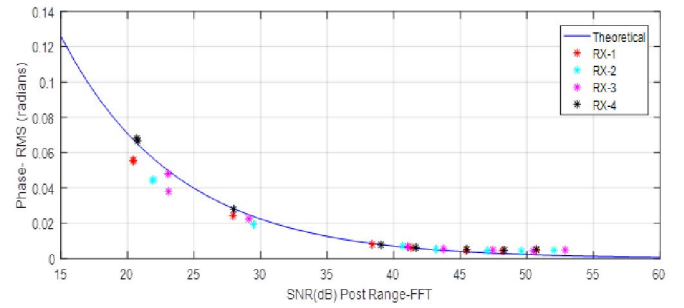

Fig. 2. Phase sensitivity measurements. Phase variations were measured at the range-bin corresponding to a static target.

We experimentally determined the phase sensitivity by measuring the phase variation across the object range-bin as a function of time for a static corner reflector placed at a fixed distance. The SNR at the object was varied by changing the transmit power. As can be seen from the plot in Figure 2 that the experimental values follow the theoretical values and at SNR > 40 dB, the phase sensitivity is < 7 milli-radians which corresponds to a displacement sensitivity of ≈ 2 microns. This gives us confidence that the system has the ability to measure tens of microns of displacements for heart-beat measurements. Further, the transmit power used to create such an antenna system can be as low as 2mW for the CMOS setup and is less than the safe exposure limits for human body towards non-ionizing radiation [5].

System Parameters			System Parameters	
Starting Frequency	77 GHz		Max. Range	4.3 m
Slow-axis Sampling	20 chirps/sec		Range Resolution	4.3 cm
Chirp Duration	50 sec		Azimuth Angular resolution	15
ADC Sampling Rate	2 Msps		Transmit Power	10 dBm

III.   PROCESSING STEPS

In this section we describe the mm-wave sensor parameters and signal processing steps involved in the extraction of the breathing-rate and heart-rate.

A. Radar Signal Acquisition Parameters

The mmwave sensor used in these experiments was a single TI-mmWave IWR1443 sensor operating at 77-81 GHz with 4 GHz chirp bandwidth [6]. The system has 3 transmit (TX) antennas and 4 receive (RX) antennas as shown in Figure 3. In order to increase the azimuth angular resolution, the chirps were transmitted in a time division multiplexing MIMO configuration by transmitting sequentially through Tx-1 and Tx-3. This results in an 8 element virtual array that gives a theoretical azimuth resolution of 15°. Some key system and chirp parameters are shown in Table 1 and described below.
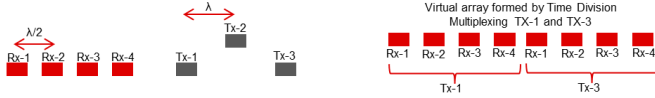

Fig. 3.   Antenna pattern on the IWR1443 EVM. Chirps were transmitted sequentially through Tx-1 and Tx-3 using time division multiplexing resulting in an 8 element virtual array

1) Slow-time axis sampling rate: The slow-axis sampling rate (chirps/second) should satisfy (a) Nyquist criteria i.e. the sampling rate should be twice the maximum frequency in the signal and to prevent any aliasing of the noise. Given that our frequency of interest is within 0.1 – 4 Hz we chose a sampling rate of 20 Hz to ensure sufficient oversampling of the signal. Moreover, (b) the sampling rate should be high enough to prevent excessive phase wrapping. For a sinusoidally vibrating object $A \sin(2\pi f_m t)$ this can be satisfied by choosing a slow-axis sampling rate such that $F_s > \frac{8\pi f_m A}{\lambda}$ where A is the amplitude and f_m is the vibration frequency.

2) Chirp Duration: The chirp duration chosen for these experiments was 50 us. In general higher the chirp duration, the better the SNR and displacement sensitivity.

3) Bandwidth: Its well known that the bandwidth of the chirp is directly related to the range resolution of the system. Although the bandwidth does not directly impact the vital signs estimation accuracy however it can significantly influence the overall performance as a higher range resolution system enables the separation of the area of interest (e.g. chest) from other limb movements and also allows better separation of one persons vital signs from another.

4) Observation Time: The larger the observation time T, the better the frequency and amplitude estimation. According to the Cramer Rao Lower Bounds (CRLB), the frequency estimation improves on the order of T^3 and amplitude estimation

by T. However, as the vital signs signals are non-stationary, the observation time is usually limited to 8 – 15 seconds due to the inherent time-frequency tradeoffs.

B. Extraction of Vital Signs Signature from Multiple People

As a first step, we need to identify the range-angle bins corresponding to the person within the radar field-of-view. Once the appropriate range-angle bins have been identified then the processing steps of Figure 4 can be applied to extract the vital signs waveform and Figure 6 to estimate the breathing-rate and heart-rate. The range-angle bin tracker runs at a user-defined time interval (e.g. every 30 seconds) and its purpose is to identify the angles of the objects of interest and then compute appropriate beam-forming weights based on these angles. Standard radar signal processing chain as outlined below is used to extract the vital signs of multiple people within the field-of-view

1) : A FMCW is transmitted over multiple TX antennas in a time division multiplexing (TDM) manner and received over several receive (RX) channels effectively forming multiple TX-RX pairs. We use a MIMO configuration to achieve better azimuth angular resolution

2) : A range-FFT is performed for each of these TX-RX pairs. This would allow objects that occupy different range bins to be separated out from one another.

3) : A second FFT is taken along the RX dimension (or other direction of arrival estimation algorithms can be used) for each of the range bins forming a range-azimuth plane. This would separate objects that fall in the same range bin but are at different angles from one another.

4) : Objects are detected in the range-azimuth plane using an object detection scheme, such as CFAR (constant false alarm rate).

5) : For each detected object in the range-azimuth plane, we measure the phase of the particular range-azimuth angle bin over the slow-time axis and only retain those range-angle bins whose phase variation over time exceeds a certain threshold (to filter out the reflections from static objects).

6) : Once the appropriate range-angle bins have been identified, beamforming weights are computed for each identified angular position k and applied to the ADC data

$$y_k[n,m] = \sum_{i=1}^{I_{Rx}} y[n,m,i] w_k^i \qquad (13)$$

7) : After the Range-FFT, the phase values are extracted from the identified range-bins and subsequently passed through a signal processing chain (shown in Figure 6) to estimate the vital signs.

C. Body Displacements Induced by Physiological Motion

At GHz frequencies, displacement of the body surface is the dominant physical mehcanism that enables non-contact vital signs measurements [7]. The body surface displacement due to breathing and heart-beat will modulate both the magnitude A_R and phase ϕ_b of the received signal. The fluctuations in A_R are most likely due to the variations in the radar cross-sectional
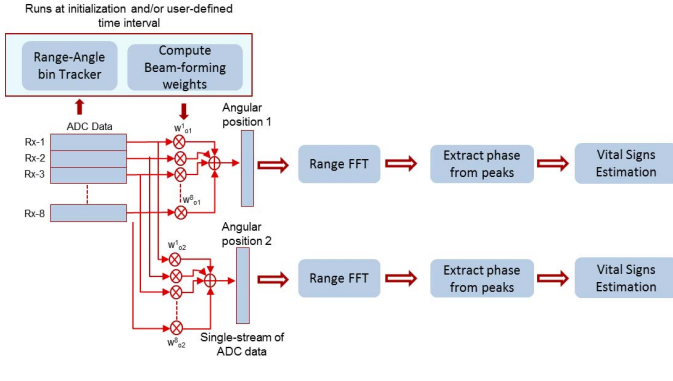
Fig. 4. Signal processing chain for separting multiple targets. Range-angle bin tracker finds the angular positions of the objects. Beamforming is subsequently performed using the weights corresponding to these angles followed by the range-FFT
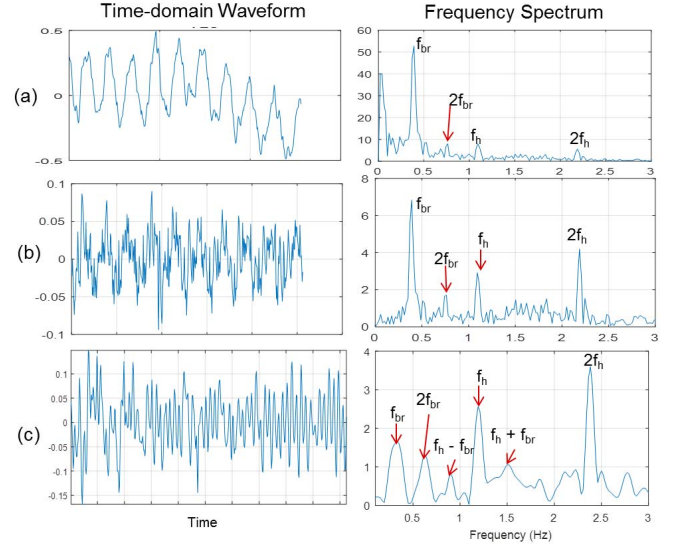

Fig. 5. Chest displacement and its frequency content (a) Unwrapped phase and its frequency content (b) Unwrapped phase after the phase difference operation. Note that the heart-rate frequencies become more obvious. (c) Another dataset of chest displacement (after phase unwrapping and difference) showing amplitude modulation of the heart-beat signal. f_{br} is the breathing-rate while f_h is the heart-rate.

(RCS) area of the human body due to displacements caused by breathing and heart-beat. In this work, we are utilizing the phase ϕ_b to extract the vibration pattern of the human chest as the phase changes are directly related to the relative changes in displacement. We also assume that the subject stays within the same angle-range bin during the measurements.

In general, the chest displacement waveforms can have significant variations depending on the spatial location of measurements, inter-person variations, state of health etc. making it difficult to come up with a general model characterizing the vital signs waveform. Some typical examples of the phase changes induced by chest displacements are shown in Figure 5. These were measured from a subject sitting stationary on a chair to minimize random body movement. From Figure 5(a), the larger amplitude displacements are due to breathing while the small oscillations on top of the breathing signal are due to heart-beats. Its immediately apparent that the chest displacement is dominated by the breathing signal which can be an order of magnitude (2x – 40x) higher than the heart-beat signal. From the frequency spectrum (right column) it can be seen that both the breathing (f_{br}) and the heart-beat (f_h) can have harmonic frequencies as these signals are rarely purely sinusoidal.

In order to minimize the impact of the larger amplitude breathing signal on the heart-rate estimate we take the phase difference between successive phase samples followed by band-pass filtering. Although this does not completely eliminate the impact of breathing and its harmonics on heart-rate estimate but nevertheless helps in enhancing the heart-rate signal. An example is shown in Figure 5(b) where the heart-rate frequency and its harmonics are more apparent. At times, the breathing harmonic frequencies can overlap with the cardiac-region spectrum (0.8 – 4.0 Hz) significantly affecting the heart-rate measurements. We also note that the heart-beat signal can be modulated by random body movement and breathing pattern. In the dataset shown in Figure 5(c), the amplitude modulation of the heart-beat signal can be observed which results in the presence of side-bands i.e. ($f_h \pm f_{br}$). The presence of all these frequency components makes picking the peak corresponding to the heart-rate difficult, but not impossible especially if intelligent DSP algorithms are employed that integrate and sift the data over many seconds of operations.

D. Signal Processing for Vital Signs Estimation

Vital signs are estimated using a running window of $T \approx$ 15 seconds. The algorithm for vital-sign estimation consists of the following main modules

1) Phase extraction and unwrapping: The phase values are computed using an arc tangent operation and unwrapped to obtain the actual displacement profile.

$$\phi(m) = unwrap[\tan^{-1}(\frac{Q}{I})] \qquad (14)$$

Subsequently, the phase differences between successive unwrapped phases are computed which helps in removing any phase drifts and in suppressing the breathing and its harmonics.

2) Noise removal: The un-wrapped differential phase $a(m)$ might be corrupted by several noise-induced phase wrapping errors especially if the phase values are close to $-\pi$ or π. This impulse-like noise is removed by computing a forward $a(m) - a(m+1)$ and backward $a(m) - a(m-1)$ phase difference for each $a(m)$ and if these exceed a certain threshold then $a(m)$ is replaced by an interpolated value.

3) Separation of breathing and heart-beat: The breathing and heart-rate occupy different frequency bands and hence can be separated by frequency filtering. A 4th order IIR-cascaded Bi-quad filter was used to bandpass the signal into the cardiac-region spectrum [0.8 - 4.0] Hz and the breathing-region spectrum [0.1 - 0.5] Hz.

4) Motion corrupted segment removal: This block reduces the impact of any large amplitude movements on the heart-rate estimates. The energy in the cardiac waveform is computed for a window size of 1 sec and if the energy E within this segment exceeds a user-defined threshold ($E > E_{Th}$), then all the samples in that segment are discarded from the time-domain cardiac waveform.

5) Windowing and gain control: Prior to spectral estimation, windowing of the signal and gain control is applied. The purpose of the gain control step is to reduce the impact of any large amplitude movements on the vital signs estimates.

6) Spectral estimation: The separated breathing and heart rate waveforms are passed through a spectral estimation module. The spectral estimation is done through the FFT algorithm.

7) Inter-peak distance: Heart-rate and breathing-rate are also estimated by finding the inter-peak distances in their respective time-domain waveforms. Two thresholds i.e. minimum peak distance (P_{min}) and maximum peak distance (P_{max}) are defined based on the sampling rate and allowed frequency range (for heart-rate this would be 0.8 - 2.0 Hz). The first peak in the waveform is chosen as a valid peak and the next valid peak is chosen such that the distance between the current peak and the previous valid peak is within the interval $[P_{min} P_{max}]$. Additionally peak can be rejected based on if their amplitudes are too high or too low based on the expected vital-signs signal amplitudes. After isolating the valid signal peaks, an estimate is made based on the average of the inter-peak distances for all the valid peaks. The inter-peak distance is used as a fallback estimate of the vital signs if the confidence metric on the FFT-based estimate is too low.

8) Breathing-Rate estimate: The breathing rate is chosen based on the frequency of the maximum-peak within the breathing-region spectrum. A confidence metric is computed as the ratio of the signal power of the maximum-peak (and some frequency bins around it) over the remaining frequency bins in the breathing-region spectrum. If confidence metric is below a certain threshold, then the inter-peak distance based estimate is chosen as the breathing-rate.

9) Heart-Rate estimate: The maximum peak in the cardiac spectrum may not necessarily correspond to the heart-rate. Breathing harmonics, noise sources, body movements, can result in larger magnitude peaks than the actual heart rate peak. Therefore we estimate the heart-rate using a density-based approach that is: find all peaks in the cardiac spectrum and retain top N peaks; remove the peaks (from the top N peaks) that correspond to breathing harmonic; place the remaining peaks in the circular buffer; accumulate the peaks for T seconds; use a clustering algorithm such as a dBscan algorithm to divide the accumulated peaks into clusters; determine the cluster with the maximum number of peaks; and choose the median peak value of the determined cluster as valid heart-rate value.
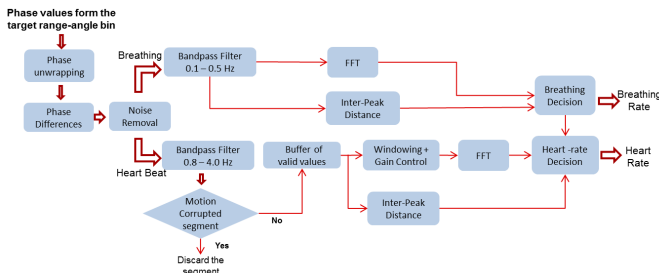

Fig. 6. Block diagram of vital signs estimation algorithm

IV. RESULTS

In the results shown in Figure 7, we placed two targets at the same range-bin but at different angles. Target 1 is a corner reflector vibrating with a fixed frequency (0.85 Hz) and amplitude (50 um) while target 2 is a person periodically breathing normally and holding the breath. As expected, when beamforming is not applied the resultant signal will be a vector summation of the two signals and the individual displacements cannot be discerned as shown in Figure 7 (a). However, after applying beam-forming the displacements from target 1 and target 2 can be clearly seen in Figure 7 (b). The separation needed between targets would depend on the range and angle resolution of the system which in our case is 4 cm and 15° respectively.
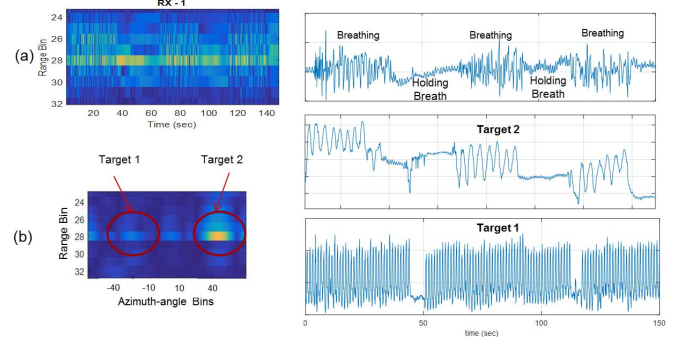

Fig. 7. Two targets placed at the same range bins but at different angles. Target 1 is a corner reflector vibrating with f = 0.85 Hz with an amplitude of 50 um while target 2 is person periodically holding his breath and breathing normally. (a) Range-profile from a single antenna. The displacement profiles of the two targets are non-discernible (b) Range-azimuth plane showing the two targets and the corresponding displacement waveforms after beamforming is used to separate the targets.

In Figure 8, we show vital signs measurements taken simultaneously from two people sitting at the same radial distance ($\approx$ 1 m) from the radar with an angular separation of $\approx 60^o$. They were asked to alternate between normal breathing and holding their breath. The separation of the chest displacement from each of these people can be seen in the plots (while one person was holding the breath the other was breathing normally).
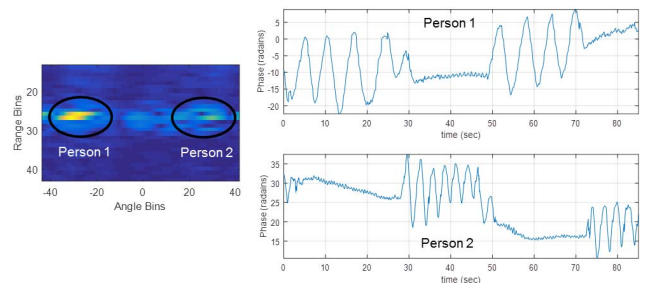

Fig. 8. Simultaneous measurement of vital signs of two people sitting at the same radial distance from the radar but at different azimuth angles. The subjects were asked to alternate between normal breathing and holding their breath and while one person was holding the breath the other was breathing normally.

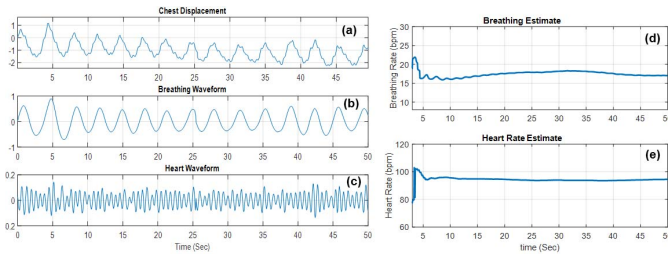Figure 9 shows an example of the breathing- and heart-

Fig. 9. Example signal waveform (a) chest displacement. Bandpass filters applied to the chest displacement to obtain the (b) Breathing waveform and (c) heart-beat waveform. (d) Breathing-rates and (e) Heart-rates estimated from the corresponding waveforms.

waveforms and breathing-rate and heart-rate obtained after applying the signal processing chain in Figure 6.

V. Conclusion and future work

Radar based non-contact vital sign monitoring has been demonstrated using several radar technologies such as UWB, CW Doppler radar and FMCW [8], [9]. While all these methods work fine under controlled environment and conditions, several challenges need to be addressed to make these systems reliable and robust enough to be deployed in real-world settings. These challenges include dealing with the impact of random body and sensor movement, effective cancellation of breathing harmonics and robust measurements in a clutter rich environment etc. In general, solving for these challenges will require more signal processing capabilities [10], [11], more radars [12] or combining radars with other sensing modalities [13], [14]. For more robust measurements and motion compensation it might be beneficial to take measurements of the same set of people from multiple overlapping view-points. This can be done for example by connecting multiple CMOS mm-wave sensors to a TDA3x embedded processor device. In addition to vital signs, mmwave sensors can potentially be used to measure drowsiness [15], stress levels [16] and human emotions [17]. Continued experimentation and research into these systems is still necessary for critical safety and emergency response applications that have been listed out in section 1 of the paper.

References

[1] J. Hasch, E. Topak, R. Schnabel, T. Zwick, R. Weigel, and C. Waldschmidt, "Millimeter-wave technology for automotive radar sensors in the 77 ghz frequency band," *IEEE Transactions on Microwave Theory and Techniques*, vol. 60, no. 3, pp. 845–860, 2012.

[2] F. Topfer and J. Oberhammer, "Millimeter-wave tissue diagnosis: The most promising fields for medical applications," *Microwave Magazine, IEEE*, vol. 16, no. 4, pp. 97–113, 2015.

[3] C. Gu, "Short-range noncontact sensors for healthcare and other emerging applications: A review," *Sensors (Basel, Switzerland)*, vol. 16, no. 8, p. 1169, 2016. [Online]. Available: http://www.ncbi.nlm.nih.gov/pmc/articles/PMC5017335/

[4] G. M. Brooker, "Understanding millimetre wave fmcw radars," in *Proc. 1st International Conference on Sensing Technology*, Palmerston North, New Zealand, 2005.

[5] Non-ionizing radiation safety manual. [Online]. Available: https://ehs.berkeley.edu/laser-safety/non-ionizing-radiation-safety-manual

[6] Texas instruments mmwave sensors. [Online]. Available: https://www.ti.com/sensing-products/mmwave/overview.html

[7] O. Aardal, Y. Paichard, S. Brovoll, T. Berger, T. S. Lande, and S. E. Hamran, "Physical working principles of medical radar," *Biomedical Engineering, IEEE Transactions on*, vol. 60, no. 4, pp. 1142–1149, 2013.

[8] F. Adib, H. Mao, Z. Kabelac, D. Katabi, and R. Miller, "Smart homes that monitor breathing and heart rate," in *Proc. 33rd Annual ACM Conference on Human Factors in Computing Systems*, Seoul, Republic of Korea, 2015.

[9] B. Schleicher, I. Nasr, A. Trasser, and H. Schumacher, "Ir-uwb radar demonstrator for ultra-fine movement detection and vital-sign monitoring," *Microwave Theory and Techniques, IEEE Transactions on*, vol. 61, no. 5, pp. 2076–2085, 2013.

[10] G. Shafiq and K. C. Veluvolu, "Surface chest motion decomposition for cardiovascular monitoring," *Sci. Rep.*, vol. 4, 2014. [Online]. Available: http://dx.doi.org/10.1038/srep05093

[11] I. Mostafanezhad, E. Yavari, O. Boric-Lubecke, V. M. Lubecke, and D. P. Mandic, "Cancellation of unwanted doppler radar sensor motion using empirical mode decomposition," *Sensors Journal, IEEE*, vol. 13, no. 5, pp. 1897–1904, 2013.

[12] L. Changzhi and L. Jenshan, "Random body movement cancellation in doppler radar vital sign detection," *Microwave Theory and Techniques, IEEE Transactions on*, vol. 56, no. 12, pp. 3143–3152, 2008.

[13] I. V. Mikhelson, P. Lee, S. Bakhtiari, T. W. Elmer, A. K. Katsaggelos, and A. V. Sahakian, "Noncontact millimeter-wave real-time detection and tracking of heart rate on an ambulatory subject," *Information Technology in Biomedicine, IEEE Transactions on*, vol. 16, no. 5, pp. 927–934, 2012.

[14] G. Changzhan, W. Guochao, L. Yiran, T. Inoue, and L. Changzhi, "A hybrid radar-camera sensing system with phase compensation for random body movement cancellation in doppler vital sign detection," *Microwave Theory and Techniques, IEEE Transactions on*, vol. 61, no. 12, pp. 4678–4688, 2013.

[15] J. Vicente, P. Laguna, A. Bartra, and R. Bailon, "Drowsiness detection using heart rate variability," *Med Biol Eng Comput*, vol. 54, no. 6, pp. 927–37, 2016.

[16] S. Suzuki, T. Matsui, H. Imuta, M. Uenoyama, H. Yura, M. Ishihara, and M. Kawakami, "A novel autonomic activation measurement method for stress monitoring: non-contact measurement of heart rate variability using a compact microwave radar," *Med Biol Eng Comput*, vol. 46, no. 7, pp. 709–714, 2008. [Online]. Available: http://dx.doi.org/10.1007/s11517-007-0298-3

[17] M. Zhao, F. Adib, and D. Katabi, "Emotion recognition using wireless signals," in *Proceedings of the 22Nd Annual International Conference on Mobile Computing and Networking*, ser. MobiCom '16. New York, NY, USA: ACM, 2016, pp. 95–108. [Online]. Available: http://doi.acm.org/10.1145/2973750.2973762